Supporting Information

Lopez et al. 10.1073/pnas.1606372113

Application of the Rod Model to Light Scattering

The scattering from a dilute solution of weakly interacting particles can be approximated by

$$\frac{Kc}{R_\theta}=\frac{1}{P(q)M_w}+2A_2c\simeq\frac{1}{M_w}\left(1+\frac{q^2\langle R_g^2\rangle_z}{3}\right)+2A_2c, \qquad [S1]$$

where $q=4\pi n_0\sin(\theta/2)/\lambda$ is the scattering vector magnitude with the scattering angle θ, the refractive index of the solvent n_0, and the wavelength of the light λ. R_θ is the excess Raleigh ratio and c is the concentration of the solute in grams per liter, K is a constant given by $K=\frac{4\pi^2n_0^2}{N_A\lambda^4}\left(\frac{dn}{dc}\right)^2$, N_A is Avogadro's number, $\left(\frac{dn}{dc}\right)$ is the refractive index increment of the solute in the solvent, $P(q)$ is the form factor, A_2 is the second virial coefficient; M_w is the weight-averaged molecular weight of the solute, defined as

$$M_w=\frac{\sum_i^\infty n_iM_i^2}{\sum_i^\infty n_iM_i},$$

where n_i is the number fraction of a species with molar mass M_i. $\langle R_g^2\rangle_z$ is the z-averaged square radius of gyration, given by

$$\langle R_g^2\rangle_z=\frac{\sum_i^\infty n_iM_i^2R_{g,i}^2}{\sum_i^\infty n_iM_i^2}.$$

Vimentin assemblies adopt a structure close to that of rigid cylinder-like particles. Hence, Eqs. **S1**–**S6** relate results from SLS to suitable model parameters. The form factor for thin rods of length L is given by (24)

$$P(q,L)=\frac{2}{qL}\int_0^\infty\sin(qL)/(qL)dL-\left(\frac{\sin(qL/2)}{(qL/2)}\right)^2.$$

For polydisperse systems, the form factor $P_z(q,L)$ is the z-average over a distribution of particle sizes,

$$P_z(q,L)=\frac{\int_0^\infty w(L)LP(q,L)dL}{\int_0^\infty w(L)LdL}, \qquad [S2]$$

where $w(L)$ is the weight distribution function of particle length L, which can be modeled by a Schultz–Zimm (SZ) function, based on the weight average of the length L_w (30),

$$w(L)=\left(\frac{z+1}{L_w}\right)^{z+1}\frac{L^z}{\Gamma(z+1)}\exp\left(-\frac{(z+1)L}{L_w}\right), \qquad [S3]$$

where Γ is the Gamma function.

The z average of the squared radius of gyration $\langle R_g^2\rangle_z$ for polydisperse thin rods following an SZ distribution is given by (30)

$$\langle R_g^2\rangle_z=\frac{(z+3)(z+2)}{(z+1)^2}\frac{L_w^2}{12}. \qquad [S4]$$

The first to third moments of the molar mass for an SZ distribution are related by

$$p.d.=\frac{M_w}{M_n}=\frac{z+1}{z};\quad \frac{M_z}{M_w}=\frac{z+2}{z+1}. \qquad [S5]$$

The second virial coefficient for cylinders of diameter d is approximated by (24)

$$A_2=\frac{N_A\pi d^2L}{4M^2}\left(1+\frac{L}{d}\left(1+\frac{d}{2L}\right)\left(1+\frac{\pi d}{2L}\right)\right). \qquad [S6]$$

Dynamic light scattering measures the intensity time correlation function $g_2(t)$:

$$g_2(q,t)=\langle I(q,t)I(q,0)\rangle/\langle I(q,t)\rangle^2.$$

$I(t,q)$ is the intensity of scattered light at time t and scattering vector magnitude q. The field autocorrelation function $g_1(t,q)$ can be calculated from $g_2(t,q)$ with the Siegert relation,

$$g_2(t,q)=1+\beta[g_1(t,q)]^2,$$

where β is a constant. For a monodisperse solute $g_1(t,q)=e^{-\Gamma t}$. Γ is referred to as the inverse decay time. Generally, a distribution of inverse decay times $(G(\Gamma))$ is expected for a polydisperse system:

$$g_1(t,q)=\int G(\Gamma)e^{-\Gamma t}d\Gamma. \qquad [S7]$$

$G(\Gamma)$ may be obtained by Laplace inversion, for example, by using the CONTIN algorithm. A simple approach (15) to extract the moments of the distribution is by a modified cumulant method, where $g_1(t,q)$ is expanded as

$$g_1(t,q)=e^{-\Gamma t}\left(1+\frac{\mu_2t^2}{2!}-\frac{\mu_3t^3}{3!}+\dots\right) \qquad [S8]$$

with Γ, μ_2, and μ_3 the first, second, and third cumulants, respectively. Due to limitations in data quality, it is common to fit $g_1(t,q)$ with only the first two cumulants.

The first cumulant Γ is used to calculate the z-averaged diffusion coefficient D_z via Eq. **2** of the main text. The second cumulant μ_2 in Eq. **S8** is the variance $(\langle\Gamma^2\rangle_z-\Gamma_z^2)$ of Γ. It can be used to calculate the polydispersity $p.d.=M_w/M_n=1+1/z$ of rod-like molecules (14):

$$\frac{M_w}{M_n}=1+\frac{\mu_2}{\Gamma^2}. \qquad [S9]$$

The z-averaged diffusion coefficient for polydisperse cylinders, where the length distribution follows the SZ formula, can be calculated using an expression analogous to Eq. **S2** with $D(L,d)$ the diffusion coefficient, in place of $P(q,L)$. The diffusion coefficient of cylinders is approximated using a formula derived by Yoshizaki and Yamakawa (25), based on an interpolation between spheroids and long cylinders,

$$D=\frac{k_BT}{3\pi\eta L}\left(\ln\left(2x-1+\left[(2x-1)^2+1\right]^{1/2}\right)+x^{-1}\left(x+\sqrt{2}-\left[(2x-1)^2+1\right]^{1/2}\right)+\frac{1}{2x}\ln\left[\frac{\left(\sqrt{2}-1\right)^2\left(1+\left[(2x-1)^2+1\right]^{1/2}\right)}{2x-1+\left[(2x-1)^2+1\right]^{1/2}}\right]\right), \qquad [S10]$$

where $x=L/d$ and d is the cylinder's diameter.

Effect of Filtering

In an effort to understand the variability of our starting solutions we performed the following experiment: 0.1 mL of a 4 g/L vimentin solution was dispensed into a cuvette without filtering, followed by 3.9 mL of filtered buffer. SLS of this sample yields a molar mass of $M_w \simeq 2.2 \times 10^6$ g/mol. The sample was further diluted with filtered solvent to 0.035 g/L and remeasured and no change was found. A Holtzer plot of this sample is shown in Fig. S1 (black crosses) along with the fit to the rod form factor (blue line). The fit was obtained leaving M_w and L_w as free parameters while z was fixed to the value obtained from cumulant analysis. The sample was then filtered through a 0.22-μm filter, resulting in a significantly less aggregated ($M_w \simeq 10^6$ g/mol) sample. The decrease in M_w is accompanied by a corresponding decrease in R_g, which yields a constant M_L within experimental error if a rigid structure is assumed. The constant value of M_L suggests a longitudinal breakage of aggregates rather than lateral disaggregation. A second filtration did not induce further disaggregation. The results of these experiments are summarized in Table S1.

Zimm Plots of Dilution Series of Vimentin in Sodium Phosphate Buffer

Preparation of solutions of tetrameric vimentin in sodium phosphate buffer turned out to result in oligomers of the tetramers. To determine whether the oligomers are stable or depend on vimentin concentration, two vimentin solutions were used as stock solutions for two dilution series. Fig. S2 shows static and dynamic Zimm plots for two dilution series, including fits to Eqs. **1** and **2** in the main text with an added term in q^4. Crucially, parameters A_2 and k_D can be obtained if the aggregation state is independent of concentration. Both series show a positive virial coefficient typical for stable entities. The stability of our solutions was further confirmed by the constant M_w observed for a sample stored in a light-scattering cuvette at room temperature for 1 wk. Further, the values of A_2 are calculated using Eq. **S6** for samples 1 and 2 as $3 \pm 1 \times 10^{-7}$ mol·L·g^{-2} and $5 \pm 2 \times 10^{-7}$ mol·L·g^{-2}, respectively, with d being extracted from Eq. **S10** integrated over the SZ distribution that was fixed at the corresponding experimental D_z, L_w, and $p.d$. These values agree with the measured values within experimental error. The agreement between measured and calculated values for A_2 suggests that no concentration-dependent aggregation occurs: If samples were significantly more aggregated as the concentration increased, an abnormally low value for A_2 would result. Conversely, if aggregation increased upon dilution, a higher than expected value of A_2 would be measured. The results of these datasets, along with those of readings at single concentrations, are summarized in Table S2. Together with the results in Table S1, these are plotted in Fig. 2 of the main text.

Evaluation of SLS and DLS Curves in Kinetic Runs

Fig. S3*A* shows the scattering intensity in the Zimm representation for the 0.07-g/L kinetic run at three different times along with the line of best fit, corresponding to Eq. **1** of the main text with $A_2 = 0$. Fig. S3*B* shows three field autocorrelation functions as squares $(g_1(t,q))^2$ taken at $q^2 = 0.00029$ nm^2 ($\theta = 80°$) for the same three times used in Fig. S3*A* along with fits to Eq. **S8**. Fig. S3*C* shows the decay time Γ as a function of q^2 for the same times used in Fig. S3*A*, along with the fit to Eq. **2** of the main text (setting $k_D = 0$).

Data Cleaning

Fig. S4 plots M_w, R_g, and R_H as a function of time for the 0.07-g/L sample discussed in the main text. Points where the scattering signal is dominated by the presence of dust, as manifested by an artificially large M_w, were omitted in Figs. 2–5 of the main text; they are indicated as blue crosses. Additionally, due to the large scatter in R_g, every five points in Fig. S4 were binned into one for R_g in Fig. 2 of the main text.

Kinetic Equations

The kinetic equations describing the reaction scheme outlined in the main text can be found in ref. 23. Pallitto and Murphy (23) consider a more complicated scheme, which reduces to our model when only the last two steps are used. This is equivalent to setting to zero all reaction constants except k_{1a} and $k_{i,j}$ in ref. 23. Further, we consider the reaction order in step one (Fig. 1 of the main text) to be equal to p, which corresponds to setting $p = q$ in the model of Pallitto and Murphy. The equations describing the time dependence of the concentration of nonlaterally assembled species f_i and laterally assembled species F_i, where the subscript refers to the longitudinal degree of polymerization (i.e., the number of length increments corresponding to the elongation by an additional tetramer in f_i or by an additional ULF in F_i), are given by

$$\frac{df_i}{dt} = -pk_n[f_i]\left(\sum_{j=1}^{\infty}[f_j]\right)^{p-1} \qquad \textbf{[S11]}$$

$$\frac{dF_i}{dt} = +k_n[f_i]\left(\sum_{j=1}^{\infty}[f_j]\right)^{p-1} - \sum_{j=1}^{\infty}k_{i,j}[F_i][F_j] + \frac{1}{2}\sum_{j=1}^{i-1}k_{j,i-j}[F_j][F_{i-j}]. \qquad \textbf{[S12]}$$

The first term in Eq. **S12** accounts for the filaments generated from lateral association of the "*f*" species. The second and third terms correspond to the loss and generation of filaments of longitudinal degree of polymerization i due to end-to-end assembly of other filaments, respectively. If a polydisperse distribution of the species f is assumed, the first term in Eq. **S12** must be interpreted carefully. Because *f*-type oligomers of any length can laterally assemble with others of different length, the laterally assembled filaments of p oligomers (which account for the first term in Eq. **S12**) will have a heterogeneous mass per unit length along the respective filament. Thus, $[F_1]$ refers to the concentration of ULFs that contain at least one oligomer f_1, set by the prefactor $[f_1]$ (outside the big brackets) in the first term of Eq. **S12**. The nature of the initially occurring f and "F" species can be adjusted to the measured values of M_w and R_g (Fig. 2 of the main text) for the sample selected. The smallest soluble vimentin unit is the tetramer, with L = 60 nm and M_w = 214,000 g/mol. Given that these are values commensurate with the observed R_g and M_w values, the discrete nature of vimentin should be considered for the evaluation of the initial state of the respective kinetic run. The effective cross-sectional diameter of tetramers and longitudinal multifolds thereof is taken to be $d_{tet} = 5$ nm (11). The diameter of ULF d_F is left as a free parameter. The end-to-end aggregation constant $k_{i,j}$ is given by the product of the sum of diffusion coefficients of two molecules $(D_i + D_j)$, the distance between centers required for a collision to occur $(R_{i,j} \simeq (L_i + L_j)/2)$, and the probability that a collision results in aggregation $p_{i,j}$. The latter was calculated by Hill (33), who predicted a scaling of $p_{i,j} \propto (\delta\omega)^2/(L_i + L_j)^2$. Combining the expressions of Hill for $p_{i,j}$ and $R_{i,j}$ and Tirado and de la Torre's (26) expression for D_i and D_j, the following relation is obtained (23),

$$k_{i,j} = 4\pi R_{i,j} p_{i,j} \left(D_i + D_j\right) = \frac{k_B T N_A (\delta\omega)^2}{3\eta} \frac{L_i + L_j}{\left(L_i + L_j\right)^2} \times \left(\frac{\ln(L_i/d_F) + 0.312 + 0.565\frac{d_F}{L_i} - 0.1\frac{d_F^2}{L_i^2}}{L_i} + \frac{\ln(L_i/d_F) + 0.312 + 0.565\frac{d_F}{L_j} - 0.1\frac{d_F^2}{L_j^2}}{L_j} \right), \quad \textbf{[S13}$$

where η is the kinematic viscosity of the solvent, k_B is the Boltzmann constant, $\delta\omega$ is the product of the maximum distance and the maximum angle at which a collision between two filaments results in aggregation, and L_i and L_j are the lengths of the reacting filaments. For simplicity $k_{i,j}$ was reduced in the model of Pallitto and Murphy (23) to

$$\overline{k_{i,j}} = \frac{k_B T N_A (\delta\omega)^2}{3\eta} \frac{1}{\bar{L}} \left(\frac{\ln(\bar{L}/d_F) + 0.312 + 0.565\frac{d_F}{\bar{L}} - 0.1\frac{d_F^2}{\bar{L}^2}}{\bar{L}} \right), \quad \textbf{[S14]}$$

where $\bar{L}$ is the number-averaged length of the F species. Eq. **S14** can be further approximated as

$$\overline{k_{i,j}} = \frac{k_B T N_A (\delta\omega)^2}{3\eta} \frac{1}{\bar{L}^1} \frac{A}{\bar{L}^{1-\mu}} = G \frac{1}{\bar{L}^{2-\mu}}, \quad \textbf{[S15]}$$

where A and μ are parameters set so that $A/\bar{L}^{1-\mu}$ closely matches the expression in large brackets in Eq. **S14**. A and μ are therefore fully set by $\bar{L}$ and d_F. As an example, for the 0.07-g/L kinetic run we use $\mu \simeq 0.4822$ and $A \simeq 1{,}206$ with $\bar{L}$ in units of decimeters. For our experiments, where $\bar{L}/d_F$ does not vary by more than an order of magnitude, using this approximation never leads to an error in $\overline{k_{i,j}}$ greater than $\simeq 3\%$.

The nth moment of the concentration of the two species is defined as

$$\lambda_{fn} = \sum_{i=0}^{\infty} i^n [f_i] \quad \text{and} \quad \lambda_{Fn} = \sum_{i=0}^{\infty} (ip)^n [F_i].$$

The equations describing the zeroth to second moments of the concentration of the nonlaterally assembled species (subscript f) and the laterally assembled species (subscript F) are given as

$$\frac{d\lambda_{f0}}{dt} = -pk_n\lambda_{f0}^p \quad \textbf{[S16]}$$

$$\frac{d\lambda_{f1}}{dt} = -pk_n\lambda_{f1}\lambda_{f0}^{p-1} \quad \textbf{[S17]}$$

$$\frac{d\lambda_{f2}}{dt} = -pk_n\lambda_{f2}\lambda_{f0}^{p-1} \quad \textbf{[S18]}$$

$$\frac{d\lambda_{F0}}{dt} = k_n\lambda_{f0}^p - \frac{1}{2}\overline{k_{i,j}}\lambda_{F0}^2 \quad \textbf{[S19]}$$

$$\frac{d\lambda_{F1}}{dt} = pk_n\lambda_{f1}\lambda_{f0}^{p-1} \quad \textbf{[S20]}$$

$$\frac{d\lambda_{F2}}{dt} = p^2k_n\lambda_{f2}\lambda_{f0}^{p-1} + \overline{k_{i,j}}\lambda_{F1}^2. \quad \textbf{[S21]}$$

The initial conditions are given by

$$\lambda_{f0}(0) = [M_f]\frac{M_{tet}}{M_{f,n}(0)}$$

$$\lambda_{f1}(0) = [M_f]$$

$$\lambda_{f2}(0) = [M_f]\frac{M_{f,w}(0)}{M_{tet}},$$

where $[M_f]$ is the total concentration of vimentin in f species expressed as (number of tetramers in initially existing f species)/liter, M_{tet} is the molar mass of a tetramer, and $M_{f,n}(0)$ and $M_{f,w}(0)$ are the number- and weight-averaged molecular weights of the f species at time 0, respectively. The starting conditions for $\lambda_{F0}(0)$, $\lambda_{F1}(0)$, and $\lambda_{F2}(0)$ are calculated in an analogous manner,

$$\lambda_{F0}(0) = \frac{[M_F]}{pn_{L,0}}$$

$$\lambda_{F1}(0) = [M_F]$$

$$\lambda_{F2}(0) = [M_F]pn_{L,0},$$

where $[M_F]$ is the total concentration of vimentin in F species expressed as (number of tetramers assembled in initially existing filaments)/liter and $n_{L,0}$ is the longitudinal degree of polymerization of the initially existing filaments F, expressed as number of ULFs per filament.

The kinetic model applied in the present work represents a special case of the process determined by Eqs. **S11** and **S12** where we assume a simple scenario to fix the initial state of our kinetic model: a bimodal population consisting of (i) tetramers and (ii) an oligomeric ULF with a longitudinal degree of polymerization of $n_{L,0}$. This leads to the simplified versions of Eqs. **S11** and **S12**,

$$\frac{df_1}{dt} = -pk_n[f_1]^p \quad \textbf{[S22]}$$

$$\frac{dF_i}{dt} = +k_n[f_1]^p\delta_{i,1} - \sum_{j=1}^{\infty}\overline{k_{i,j}}[F_i][F_j] + \frac{1}{2}\sum_{j=1}^{i-1}\overline{k_{j,i-j}}[F_j][F_{i-j}], \quad \textbf{[S23]}$$

where $\delta_{i,1}$ is the Kronecker delta function, and to the simple starting conditions for the f species of $M_{f,n}(0) = M_{f,w}(0) = M_{tet}$ and $\lambda_{f0}(0) = \lambda_{f1}(0) = \lambda_{f2}(0) = [M_f]$. Eqs. **S16–S21** and the starting conditions for $\lambda_{F0}(0)$, $\lambda_{F1}(0)$, and $\lambda_{F2}(0)$ remain unaffected. The mass per unit length of the ULFs generated by the lateral assembly of tetramers is p times that of a tetramer. The scenario outlined above is capable of reproducing the R_g vs. M_w results collected in Fig. 2 of the main text. The number fraction of oligomeric ULFs is approximately constant at 0.5% (corresponding to mass fractions of 2% for the least aggregated samples and $\simeq 10\%$ for the more aggregated ones) and the variation in M_w and R_g is caused by the degree of longitudinal assembly of filaments. For the three samples used for kinetic runs in the main text, the longitudinal degree of polymerization of the filaments present at $t = 0$ is $n_{L,0} = 3$. The mass fractions of filaments at $t = 0$ are 2.3% for the 0.09-g/L sample, 2.4% for the 0.07-g/L sample, and 7% for the 0.06-g/L sample.

M_w for the entire ensemble is calculated from

$$M_w = \frac{\lambda_{F2} + \lambda_{f2}}{\lambda_{F1} + \lambda_{f1}} M_{tet},$$

which allows us to fit M_w data obtained from light-scattering experiments with the above model.

To be able to also fit $\langle R_g^2 \rangle_z$, we assume that the filaments of species F are distributed according to the SZ formula (Eq. **S3**). The polydispersity of the filament population is calculated using

$$p.d. = \frac{\lambda_{F2}\lambda_{F0}}{\lambda_{F1}^2}.$$

Once the polydispersity is known, the z-averaged square radius of gyration for each population can be calculated according to Eq. **S4**. The z-averaged squared radii of gyration for the f and F species are $R_{g,f}^2$ and $R_{g,F}^2$, respectively. We note that in the scenario applied in the present work $R_{g,f}^2 = 17$ nm (pure tetramers) and independent of time. Due to the partial overlap between ULFs, the mass per unit length of the filaments M_L, which is required to calculate $R_{g,F}^2$, is a function of the filament length L_F. We approximate the weight-averaged length of the filaments $L_{w,F}$ as M_w/M_L, where M_L is the average mass per unit length of the ensemble at a given time. M_L is given by $M_w/(63 + 43(n_L - 1))$ nm, where n_L is the longitudinal degree of polymerization for the filaments at an arbitrary time. For nondiscrete values of n_L polynomial interpolation is used. The z-averaged square radius of gyration for the entire ensemble, which is measured by static light scattering, is given by

$$\langle R_g^2 \rangle_z = \frac{\lambda_{F2} R_{g,F}^2 + \lambda_{f2} R_{g,f}^2}{\lambda_{f2} + \lambda_{F2}}.$$

The z-averaged diffusion coefficient for the f species $D_{f,z}$ and for the F species $D_{F,z}$ can be calculated by integrating Eq. **S10** over the length distribution [in an analogous way to Eq. **S2** with $D(L)$ instead of $P(q,L)$]. This requires input of the weight-averaged lengths for the tetramer and filaments $L_{f,w}$ and $L_{F,w}$, respectively, and the polydispersities for both populations. The z-averaged diffusion coefficient for the full ensemble can be calculated as

$$D_z = \frac{\lambda_{f2} D_{f,z} + \lambda_{F2} D_{F,z}}{\lambda_{f,2} + \lambda_{F,2}}.$$

Eqs. **S16–S21** cannot, to the best of our knowledge, be solved analytically for the general case of finite k_n and $\overline{k_{i,j}} \neq 0$. For the special case where end-to-end elongation does not take place ($\overline{k_{i,j}} = 0$), the above equations can be solved to give

$$\lambda_{f0} = \left(\lambda_{f0}(0)^{-p}\left[k_n p(p-1)t\lambda_{f0}(0)^p + \lambda_{f0}(0)\right]\right)^{1/(1-p)} \quad \textbf{[S24]}$$

$$\lambda_{f1} = \left(\lambda_{f1}(0)^{-p}\left[k_n p(p-1)\lambda_{f0}(0)^{p-1}\lambda_{f1}(0)t + \lambda_{f1}(0)\right]\right)^{1/(1-p)} \quad \textbf{[S25]}$$

$$\lambda_{f2} = \left(\lambda_{f2}(0)^{-p}\left[k_n p(p-1)\lambda_{f0}(0)^{p-1}\lambda_{f2}(0)t + \lambda_{f2}(0)\right]\right)^{\frac{1}{1-p}} \quad \textbf{[S26]}$$

$$\lambda_{F0} = \left(\lambda_{f0}(0) - \lambda_{f0}\right)/p + \lambda_{F0}(0) \quad \textbf{[S27]}$$

$$\lambda_{F1} = \lambda_{f0}(0) - \lambda_{f0} + \lambda_{F1}(0) \quad \textbf{[S28]}$$

$$\lambda_{F2} = \left(\lambda_{f0}(0) - \lambda_{f0}\right)p + \lambda_{F2}(0). \quad \textbf{[S29]}$$

We can also obtain an analytical solution when $k_n = \infty$. The initial conditions have to be changed to reflect the initial population of laterally assembled filaments. The analytical expressions for λ_{F0}, λ_{F1}, and λ_{F2} are then given by

$$\lambda_{F0} = \left[\left(\frac{M_L}{M_{\mathrm{ULF}}\lambda_{F1}}\right)^{2+\mu}\frac{G}{2}(\mu+3)t + \lambda_{F0}(0)^{-(\mu+3)}\right]^{-1/(\mu+3)} \quad \textbf{[S30]}$$

$$\lambda_{F1} = \lambda_{F1}(0) \quad \textbf{[S31]}$$

$$\lambda_{F2} = \lambda_{F2}(0) + H\left((J+It)^{m+1} - J^{m+1}\right)\Big/\left(I(m+1)\right), \quad \textbf{[S32]}$$

where

$$m = -\frac{2+\mu}{3+\mu}$$

$$H = G\lambda_{F2}(0)^{-\mu}M_L^{2+\mu}$$

$$I = (M_L/(M_{\mathrm{ULF}}L_{F1}(0)))^{2+\mu}G(\mu/2+1.5)$$

$$J = L_{F0}(0)^{-\mu-3}$$

$$G = \frac{k_B T N_A}{3\eta}A(\delta\omega)^2.$$

To fit data, we solve Eqs. **S16–S21** and **S15** numerically, using a Runge–Kutta 4 method implemented in Igor Pro v6.36. The time step was varied depending on sample and fit parameters between 0.03 s and 0.01 ms. We use the values of p and k_n obtained from first fitting Eqs. **S24–S29** as our starting guesses. The initial conditions are obtained from the values of M_w and $\langle R_g^2 \rangle_z$ measured for the sample before salt addition. We did not implement a least-squares minimization routine; rather, the parameters were adjusted by eye until they gave a good fit to the data. This typically took on the order of 20 iterations.

Multiplicity of Fits

Fig. S5 shows fits to M_w and R_g for the 0.07-g/L sample discussed in the main text. The parameter p was fixed to 5, 6, and 7 and k_n and $\delta\omega$ were adjusted to fit the M_w data for $t \leq 100$ min (before precipitation). Whereas the quality of the fits to M_w remains similar for all three p values, the fits to R_g vary considerably, and $p = 6$ yields the best fit to the R_g vs. t data. We note here that the calculated value of R_g initially decreases as step one proceeds. The reason for this is that when tetramers assemble laterally to form a ULF, their relative contribution to R_g increases and therefore the relative contribution of the longer species (trimers F_3 in this case) decreases. This decrease occurs only at very early times; R_g then levels off and eventually increases due to end-to-end elongation. Our data do not permit checking this feature of our model.

Justification of Number of Free Parameters and Alternative Fit

Number of Free Parameters. The model presented uses four free parameters: two reaction constants k_n and $\delta\omega$, one for each reaction step; the degree of laterally assembled tetramers in filaments, p (or alternatively the mass per unit length M_L of the filaments); and one hydrodynamic parameter, d_F. We judge this to be an appropriate number of free parameters relative to the amount of data presented. A minimum of two reaction constants are required to model a two-step process and p is fully determined by the correlation between M_w and R_g. Further, a hydrodynamic

diameter (which is not available from the literature and is expected to deviate significantly from the cross-sectional diameter measured by electron microscopy or calculated from p or M_L) is required to fit the R_H vs. time data. Once the optimized value of d_F is obtained, we rerun the procedure outlined in *Supporting Information*, *Multiplicity of Fits* for M_w and R_g and find that using this new value has virtually no effect on the quality of the fits. d_F is therefore independently set by the R_H vs. time data. Compared with other techniques such as UV-Vis spectroscopy, which measures concentrations of filaments, or electron microscopy, which typically yields the relative length (and/or width) distribution of filaments (without having access to absolute concentrations of a given species), combined SLS/DLS provides mass, structural, and hydrodynamic data on an absolute scale. As explained in *Supporting Information*, *Multiplicity of Fits*, if one considers only one of either parameter M_w or R_g, for example M_w, p can be set to any reasonable value without the fit being significantly affected. Availability of both M_w and R_g from SLS resolves a final value for p. If R_g is obtained from electron microscopy images at variable time, its kinetic interpretation, which has to be inevitably based on monomer loss and particle growth in terms of mass values, requires an additional guess on the mass per unit filament length.

In conclusion, the different parameters are set by either independent datasets (p and d_F) or different time regions (k_n and $\delta\omega$). Compared with other techniques commonly used to study protein self-assembly, time-resolved–SLS/DLS yields relatively extensive datasets where different quantities (mass, length, and diffusion) are measured.

Use of a Modified Exponent Fit. The fit presented in the main text was carried out with as few free parameters as possible, with deviations of the fit from experimental data not larger than 20% (except for R_g recorded at very early times where the scatter in the data is large). We now consider the inclusion of an additional free parameter to improve the agreement with our data. Hill (33) estimated the probability that a collision between two rods with lengths L_i and L_j results in aggregation as $p_{i,j} \propto (\delta\omega)^2/(L_i+L_j)^2$. In his calculation, rotational motions of rods and intermolecular excluded volume were neglected. Even if his calculation is exact for rods, the predicted scaling may be modified if additional interactions like, for instance, electrostatic or van der Waals interactions exist between the ends of two rods. It therefore seems possible that the true exponent for $p_{i,j}$ could deviate significantly from Hill's (33) value of 2. We have therefore also fitted our data using $p_{i,j} \propto (\delta\omega)^2/(L_i+L_j)^{\alpha}$, where α is left as a free parameter. The best-fit value of $\alpha = 3.5$ significantly deviates from Hill's prediction and yields a correct description of M_w, R_g, and R_H as a function of time, shown in Fig. S6. All data (M_w, R_g, and R_H) in the elongation-dominated regime ($t \geq 5$ min) never deviate by more than 10% from the fit. The deviation of the exponent can be interpreted as a length dependence of $\delta\omega$, meaning that the maximum distance or angle between two colliding rods decreases with rod length as $\sim L^{-0.75}$. An exponent of $\alpha = 4$ would have a simple geometrical interpretation: A sphere with diameter L is drawn around each of the reacting filaments involved in an elongation step. Along with this, two identical surface areas (independent of rod length) are fixed at opposing sides of each sphere corresponding approximately to the ends of the rods. A collision between these spheres results in aggregation when the two drawn surface areas contact without the spheres overlapping. This schematic leads to a dependence on length of the maximum angle between rods for a successful collision of $\omega \sim 1/L$ and $p_{i,j} \sim 1/(L^4)$ and thus to an exponent of $\alpha = 4$. However, we consider the addition of this parameter as a first hint for a more complicated elongation mechanism as has been so far applied and therefore we have opted to present the fit with $\alpha = 3.5$ in Fig. S6 as an alternative fit to the one of the more simple model shown in the main text.

Comparison with Literature Data. Portet (34) carefully analyzed the filament length distribution data of vimentin at several times in the interval of 60–14,400 s in 0.1 M KCl at 37 °C by means of images from electron microscopy, atomic force microscopy, and total internal reflection fluorescence microscopy. Fits with a model similar to ours yielded an elongation rate constant [$\hat{p}$ for model I in ref. 34, which is equivalent to $(\delta\omega)^2/8$ in our model] that increased with increasing reaction time, which is similar to using an exponent of $\alpha < 2$. This trend is opposite to our modified fit where a best fit is obtained with $\alpha = 3.5$, corresponding to a $\delta\omega = \sqrt{8\hat{p}}$ [in the terminology of Portet (34)] decreasing with time. Although we do not know the cause of this disagreement, it is worth noting that both studies suggest that the elongation step for vimentin is more complex than simple end-to-end aggregating rods.

Variability with Concentration

Fig. S7*A* shows M_w vs. time for the three different concentrations studied. A significant variation in the kinetics between the 0.07-g/L and the 0.09-g/L samples can be observed. Fig. S7*B* shows a plot of R_g vs. M_w for the three kinetic runs, along with limiting power laws of $R_g = kM_w^1$, which is the functional form expected for rigid rods of constant polydispersity. The mass per unit length determines the value of k given a value for the polydispersity. The aggregation process remains qualitatively the same for all samples as seen in Fig. S7 *C* and *D*: First, a lateral aggregation step occurs, signaled by a large increase in M_w without any significant increase of R_g. Eventually, the increase in R_g coupled with an increase in the ρ parameter signals elongation, with a $M_w \propto t^{1/3}$ characteristic for end-to-end association of rods. Fig. S7*B* shows that the mass per unit length for the 0.09 sample is $\simeq$ 1.5 times and 1.8 times larger than those for the 0.07-g/L and 0.06-g/L samples, respectively. This difference could be due to an error in the determination of concentration of our protein solutions, which in turn affects the calculated values of M_w (but not R_g). Specifically, if the actual concentrations for the 0.06-g/L and 0.07-g/L samples are 30–40% lower than the value we used for our calculations, and the concentration of the 0.09-g/L sample is 30% higher, the three curves overlay and the p values obtained from our model fits coincide for all three samples, giving within experimental uncertainty $p =$ 7–8, in agreement with previous reports (4). The fits shown in Fig. S7 *C* and *D* refer to the experimentally determined protein concentration; however, the quality of the fits to M_w or R_g is not affected significantly by a change of 30% in the assumed concentration set to make all M_w trends compatible with a unique $p = 8$.

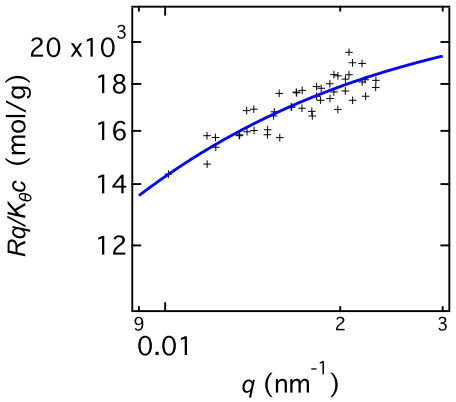

Fig. S1. Holtzer plot for the sample without filtering corresponding to the highest M_w and R_g in Fig. 2 of the main text. Blue line indicates the fit to the polydisperse rod form factor.

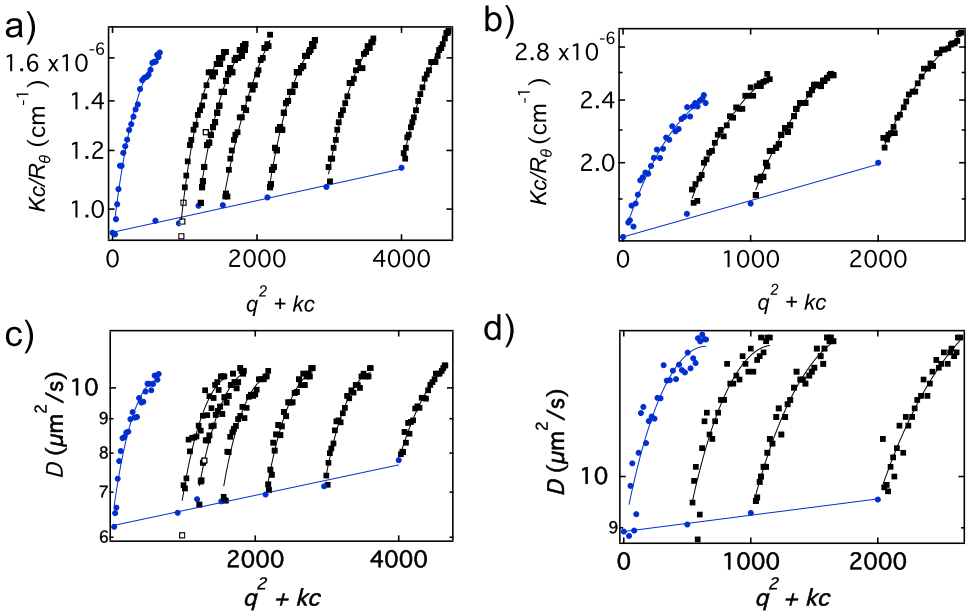

Fig. S2. Static (*A* and *B*) and dynamic (*C* and *D*) Zimm plots for two vimentin samples in sodium phosphate buffer. Shown are sample 1 (*B* and *D*) and sample 2 (*A* and *C*) (details in Table S2). Squares represent data points and circles represent values extrapolated to zero concentration. Lines are quadratic fits to the data. Open symbols are deleted points. *k* is an arbitrary constant set to 4,000 for sample 1 and to 20,000 for sample 2.

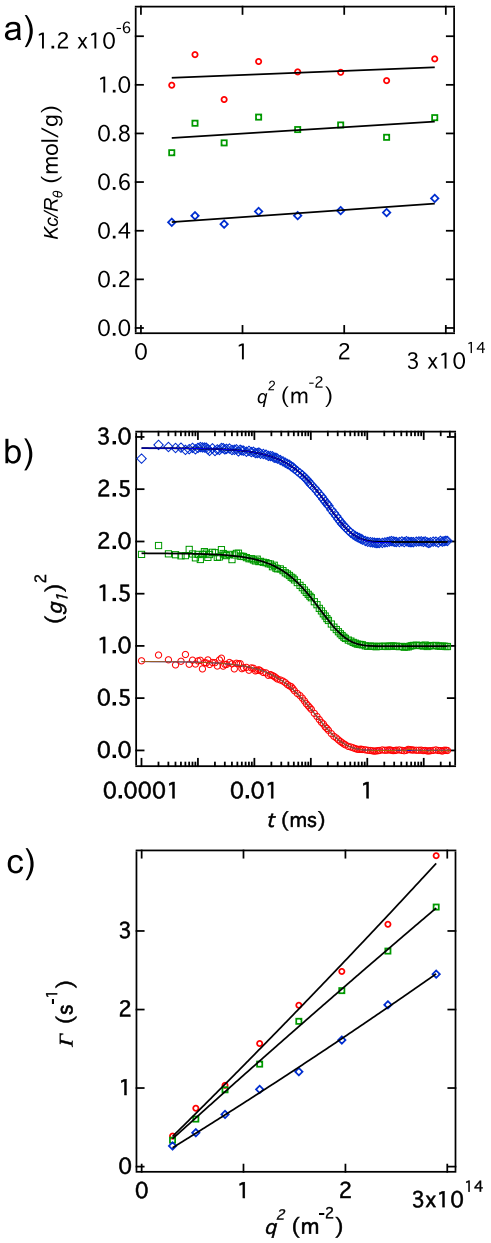

Fig. S3. Color code: red symbols, $t = 0.5$ min; green symbols, $t = 2$ min; blue symbols, $t = 35$ min. (*A*) SLS data in the Zimm representation. Lines are fits to Eq. **1** of the main text. (*B*) Square of the electric field time correlation functions $g_1(t)^2$. Correlation functions at angle 80° along with fits to Eq. **S8**. Green and blue curves are shifted vertically by values of 1 and 2, respectively, for clarity. (*C*) Decay time Γ vs. q^2 along with fits to Eq. **2** of the main text.

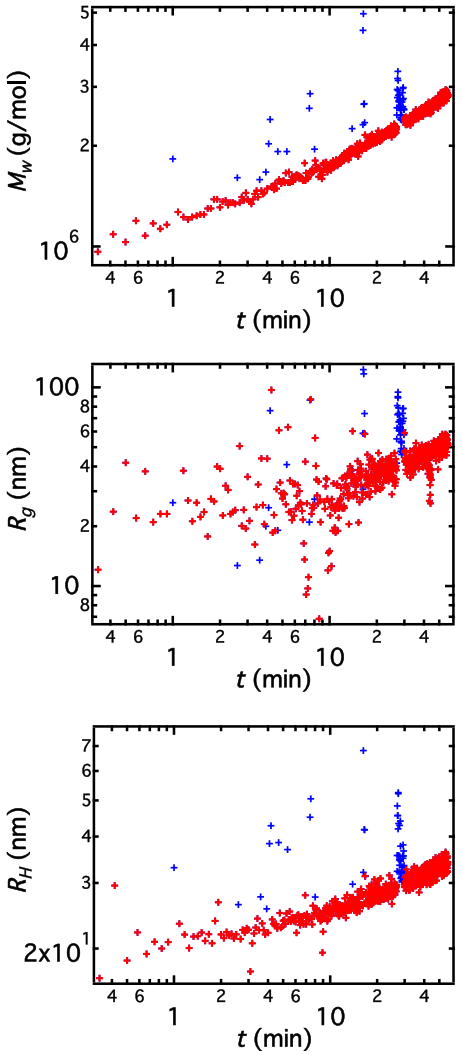

Fig. S4. M_w, R_g, and R_H as a function of time for the 0.07-g/L vimentin sample discussed in the main text. Blue points correspond to the deleted data points and red points to the data presented in the main text.

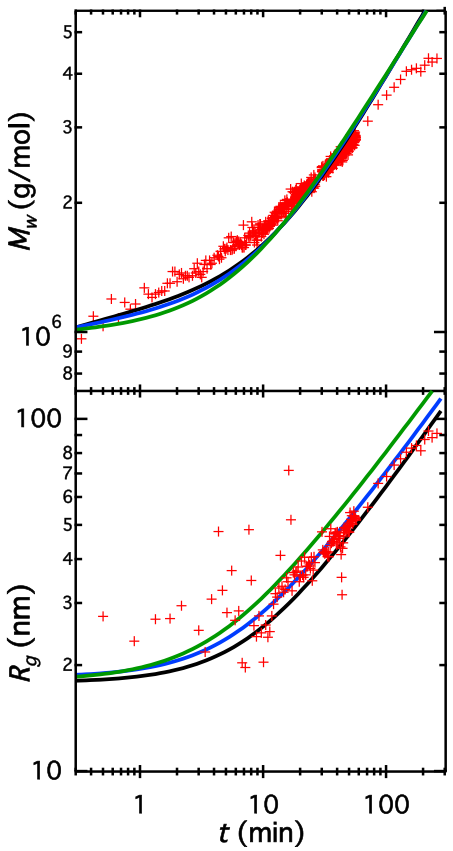

Fig. S5. Fit according to the kinetic model. Red symbols show M_w vs. time (*Top*) and R_g vs. time (*Bottom*) for the kinetic run at vimentin concentration of 0.07 g/L. Lines are fits to the model presented in the main text. Green line, $p = 5$; blue line, $p = 6$; black line, $p = 7$. k_n and $\delta\omega$ are adjusted to yield a best fit to the M_w data for $t \leq 100$ min.

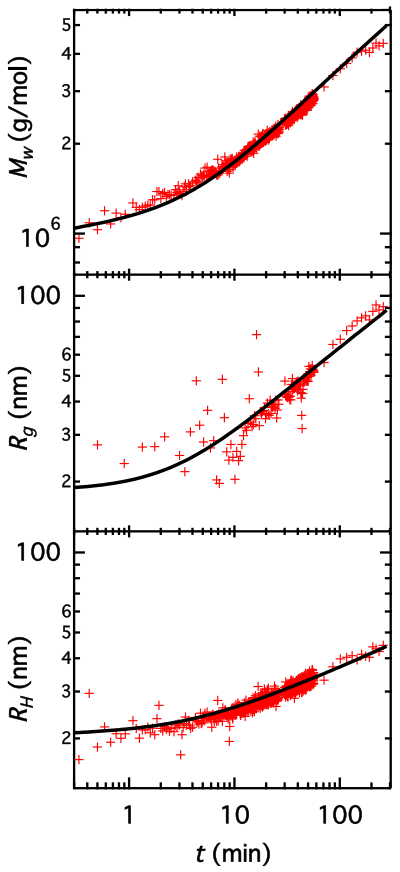

Fig. S6. Fit with modified $\alpha = 3.5$ and $p = 6$. Symbols and lines have the same meaning as in Fig. 5 of the main text.

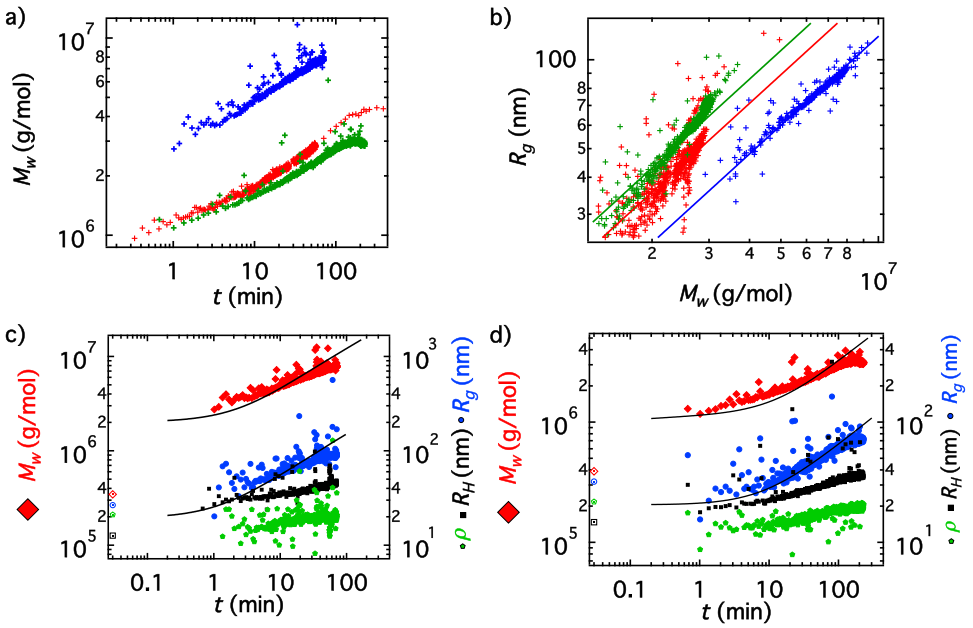

Fig. S7. (*A*) M_w vs. time for three different kinetic runs. Blue symbols, $c = 0.09$ g/L; red symbols, $c = 0.07$ g/L; green symbols, $c = 0.06$ g/L. (*B*) R_g vs. M_w. Symbols have the same meaning as in *A*. (*C*) M_w (red diamonds), R_g (blue circles), R_H (black squares), and $\rho \times 10$ (green stars) for the kinetic run with vimentin concentration of 0.09 g/L. Large open symbols at $t = 0.03$ min represent values before addition of KCl. (*D*) Same as *C* but for 0.06-g/L vimentin concentration. The lines in *C* and *D* represent fits with the kinetic model applied in the same way as done for $c = 0.07$ g/L in Fig. 5 and Fig. S5. The results from all fits are summarized in Table 1 of the main text.

Table S1. Effect of filtering

Sample	R_g, nm	M_w, g/mol	R_H, nm	C	$p.d.$	M_L*, kg·mol^{-1}·nm^{-1}	c, g/L
Not filtered	140 ± 30	2.2 ± 0.3 × 10^6	63 ± 7	0.22 ± 0.05	2.2 ± 0.1	6.9 ± 2	0.098–0.035†
Filtered	52 ± 10	9.2 ± 0.1 × 10^5	31 ± 1	0.3 ± 0.1	1.8 ± 0.1	9 ± 2	0.035
Refiltered	56 ± 5	9.2 ± 0.1 × 10^5	33 ±2	0.35 ± 0.1	1.8 ± 0.1	8.6 ± 0.9	0.035

*$M_L = M_w/L_w$.
†A first measurement was taken at 0.098 g/L, and the solution was then diluted to 0.035 g/L and remeasured. Values correspond to the average between the two readings.

Table S2. The parameters from Zimm analysis for two vimentin samples studied as a function of concentration (first two rows) and the parameters measured at a single concentration (other rows)

Sample	R_g, nm	M_w, g/mol	L_w, nm	R_H, nm	C	ρ	M_L, kg·mol^{-1}·nm^{-1}	A_2, mol·L·g^{-2}	k_D, dm^3/g	$p.d.$	c, g/L
Dilution 1	58 ± 3	6.1 ± 0.3 × 10^5	115 ± 4	26 ± 5	0.34 ± 0.05	2.3 ± 0.5	5.3 ± 0.5	2.4 ± 0.6 × 10^{-7}	—	1.5	0.5–0.13
Dilution 2	73 ± 2	1.1 ± 0.1 × 10^6	220 ± 10	37 ± 3	0.26 ± 0.05	2 ± 0.2	6.3 ± 0.5	5.5 ± 0.3 × 10^{-7}	1.2 ± 0.3	1.5	0.2–0.046
Sample 1	25 ± 6	3.2 ± 0.2 × 10^5	60 ± 10	14 ± 1	0.17 ± 0.06	1.8 ± 0.6	5 ± 1	—	—	1.3	0.14
Sample 2	32 ± 3	4.5 ± 0.1 × 10^5	84 ± 6	15 ± 1	0.20 ± 0.03	2.2 ± 0.3	6 ± 1	—	—	1.5	0.12
Sample 3	28 ± 5	3.9 ± 0.4 × 10^5	70 ± 14	13 ± 1	0.22 ± 0.05	2.1 ± 0.6	6 ± 1	—	—	1.3	0.12
Sample 4	27 ± 2	3.5 ± 0.3 × 10^5	66 ± 6	12.6 ± 0.5	0.2 ± 0.04	2.1 ± 0.3	5 ± 1	—	—	1.4	0.18
Sample 5	100 ± 10	1.9 ± 0.2 × 10^6	220 ± 20	52 ± 5	0.2 ± 0.05	2.0 ± 0.4	8.6 ± 0.1	—	—	1.8	0.18
Sample 6	58 ± 4	1.0 ± 0.1 × 10^6	120 ± 10	38 ± 3	0.32 ± 0.09	1.5 ± 0.2	6.3 ± 0.5	—	—	1.8	0.2
Sample 7	55 ± 4	1.2 ± 0.1 × 10^6	120 ± 10	36 ± 3	0.32 ± 0.07	1.5 ± 0.2	6.3 ± 0.5	—	—	1.8	0.2
Sample 8	56 ± 4	1.2 ± 0.1 × 10^6	120 ± 10	36 ± 3	0.32 ± 0.05	1.5 ± 0.2	6.3 ± 0.5	—	—	1.8	0.2

In column 3, L_w is calculated via Eq. **S4** and the mass per unit length in column 7 is set to $M_L = M_w/L_w$.